Wide-angle AVO waveform inversion with WKBJ modeling

Rodrigo Felicio Fuck*, Chris H. Chapman and Colin Thomson, Schlumberger Cambridge Research,UK

Abstract

We propose a new target-oriented inversion workflow aimed at extending AVO-type inversions to long-offset seismic data. Such an ability improves reservoir parameter estimation, allowing sharper discrimination of velocity and density changes across an interface in comparison with estimations done with AVO inversion based on plane-wave reflection coefficients. The forward modeling used during the inversion is the WKBJ seismogram algorithm, a fast and robust way to compute seismograms from pre-critical partial reflections, through transitional waveforms, which include the interference with head waves, to total-reflection signals. The inversion fits a target reflection in raw shot or CMP gathers by direct comparison of either the waveforms of the observed data and modeled WKBJ seismograms or of their respective envelopes. In addition, to avoid local minima the workflow has been divided into two stages: first, a global random search of the parameter space provides the initial model, which is then fed into the second stage, a local gradient-based optimization. Inversions of a synthetic model and a raw shot gather from a 2D point-receiver survey demonstrate that the inclusion of wider-angle, near-critical and post-critical data in the proposed inversion improves the resolution of both velocity and density contrasts.

Introduction

The industry standard procedure for estimation of reservoir parameters from reflection seismic data is to use the amplitude variation with offset (AVO) of target events. Typically, AVO-type inversions rely on two key assumptions: a 1D earth model and the representation of the amplitude variations using reflection coefficients of plane waves, which may be obtained from Zoeppritz's equations (Aki and Richards, 2002) or approximations of them for isotropic (Shuey, 1985) and anisotropic media (Rüger, 1997). In practice, the assumption of plane waves restricts the offset range that can be input into the inversion. Indeed, near-critical and postcritical reflections, which usually occur on long offsets, cannot be accurately modeled, because the interference of head waves can only be accounted for if the incident wavefront is curved (Chapman, 2004). Unfortunately, such limitation of the offset range is at the root of the inherent inability of AVO inversions to decode P- and S-wave impedances into robust estimates of density and body wave velocity contrasts across an interface (van der Baan and Smit, 2006).

We remove the plane-wave limitation by using WKBJ seismograms to model seismic signals from a target reflector. These seismograms are constructed from ray-traced quantities, but can account for nongeometric propagation phenomena, like the head wave and its interference with the reflected signal around the critical offset. Hence, the WKBJ algorithm allows the AVO inversion to be carried out using data from near traces, with only partial reflections, to beyond the critical offset trace, where the incident waveform is totally reflected. Other attractive features of WKBJ seismograms are computational cost and the output of band-limited signals. For instance, the cost of synthesizing WKBJ seismograms is proportional to a linear combination the number of output samples n_t and the number of slownesses (or plane-waves) used in the computations, n_p. In contrast, the cost of seismograms computed using a reflectivity algorithm is proportional $n_t \times n_p$. Contrary to inversions based on effective reflection coefficients for spherical waves (Ursenbach et al., 2007), the WKBJ algorithm delivers band-limited seismograms that can be directly compared to the data, with no need for an intermediate step to map input seismic traces in time and offset domain into reflection coefficients as a function of angle of incidence. In addition, the WKBJ algorithm does not assume isotropy, so it can be used for anisotropic inversions as well.

WKBJ seismogram algorithm

This modeling algorithm, introduced by Chapman (1978), uses the WKBJ method (after Wentzel, Kramer, Brillouin and Jeffreys) to find asymptotic approximations to the particle velocity Green function in the frequency-wavenumber (or ray parameter) domain. By transforming such a response to the time-space domain, one obtains the impulse response of a seismic point source in a 1D earth. In essence, the WKBJ seismogram algorithm results from doing such a transformation analytically.

By requiring that no evanescent waves impinge on the reflecting interface (i.e., the time intercept function is assumed real), and further assuming that receivers are in the far field, the WKBJ solution for the displacement impulse response of a given ray type (e.g., for a reflection or any of its multiples), $\underline{\mathbf{u}}_{\text{ray}}$, for each time t and each receiver Cartesian location $\mathbf{x}_{\text{R}}$ —in 3D geometry, but for a 1D earth model— is found to be (Chapman, 2004):

$$\underline{\mathbf{u}}_{\text{ray}}(t,\mathbf{x}_{\text{R}}) = -\frac{1}{2^{3/2}\pi^2 x_{\text{R}}^{1/2}} \times \frac{\mathrm{d}}{\mathrm{d}t}\mathrm{Im}\left(\Lambda(t) * \sum_{\widetilde{T}_{\text{ray}}=t} \frac{p^{1/2}\underline{\mathscr{G}}_{\text{ray}}(p)}{|\partial \widetilde{T}_{\text{ray}}/\partial p|}\right). \quad (1)$$

Above, p is the horizontal slowness component characterizing a plane wave and $\widetilde{T}_{\text{ray}}$ is the traveltime function for such a plane wave between a given source-receiver pair. This function equals the geometric ray traveltime T_{ray}, if the receiver radial position x_{R} coincides with the range of the geometrical arrival X_{ray}. More generally,

$$\widetilde{T}_{\text{ray}}(p, z_{\text{R}}) = T_{\text{ray}}(p, z_{\text{R}}) + p\,[x_{\text{R}} - X_{\text{ray}}(p, z_{\text{R}})]\,, \qquad (2)$$

where z_{R} is the receiver depth. The main contributions to the summation in equation 1 come from the extrema of the function $\widetilde{T}_{\text{ray}}$, which correspond to geometrical arrivals. These contributions, in turn, are scaled up by the propagation dyadic $\underline{\mathscr{G}}_{\text{ray}}(p)$ that encodes the polarization vectors at the source ($\mathbf{g}_{\text{S}}$) and receiver ($\mathbf{g}_{\text{R}}$) for a given p, and the appropriate plane-wave reflection and transmissions coefficients, $\mathscr{T}_{ij}$, along a ray:

$$\underline{\mathscr{G}}_{\text{ray}}(p) = \left(\prod_{\text{ray}} \mathscr{T}_{ij}(p)\right) \mathbf{g}_{\text{R}}(p)\mathbf{g}_{\text{S}}^{\text{T}}(p)\,. \qquad (3)$$

The final shape of the impulse response seismograms—with delta functions or their Hilbert transforms marking the geometric arrivals—is obtained by convolution with the operator $\frac{\text{d}}{\text{d}t}\text{Im}[\Lambda(t)]$, where $\Lambda(t) = \lambda(t) + i\overline{\lambda}(t) = t^{-\frac{1}{2}}$ is an analytic signal; Im is the imaginary part, and $i^2 = -1$. Note that equation 1 cannot be used to simulate short offsets or a VSP experiment (i.e., when $x_{\text{R}} \approx 0$).

In practice, it is necessary to regularize equation 1 before computation of synthetics, because of singularities associated with $|\partial \widetilde{T}_{\text{ray}}/\partial p| = 0$. Therefore, Chapman (1978) suggests smoothing expression 1 with a time-domain boxcar filter that is twice as long as the sampling interval of the seismogram, Δt, i.e., $B(t/\Delta t)/\Delta t$, where

$$B(t) = \frac{1}{2}\,[H(t+1) - H(t-1)] \qquad (4)$$

and $H(t)$ is the Heaviside step function. Then equation 1 is rewritten as

$$\frac{B(t/\Delta t)}{\Delta t} * \underline{\mathbf{u}}_{\text{ray}}(t, \mathbf{x}_{\text{R}}) \approx -\frac{1}{2^{3/2}\pi^2 x_{\text{R}}^{1/2}\Delta t} \times \frac{\text{d}}{\text{d}t}\text{Im}\left(\Lambda(t) * \sum_{\widetilde{T}_{\text{ray}} = t \pm \Delta t} \int p^{1/2}\underline{\mathscr{G}}_{\text{ray}}(p)\text{d}p\right). \qquad (5)$$

The integrals are evaluated over the narrow slownesses intervals defined by $\widetilde{T}_{\text{ray}} = t \pm \Delta t$ and then summed to obtain the amplitude for a given time sample t. As observed by Chapman (2004), the convolution with the boxcar not only stabilizes the computation of the time series, but also diminishes the errors caused by interpolation of the functions $\underline{\mathscr{G}}_{\text{ray}}(p)$ and $\widetilde{T}_{\text{ray}}(p, \mathbf{x}_{\text{R}})$. Furthermore, such convolution allows rapid linear interpolation of the integrand and integration using trapezoidal rule, making computations cheap and efficient.

Inversion workflow

The proposed workflow puts in place a nonlinear, least-squares waveform inversion. Following Cary and Chapman (1988), we subdivided the inversion into two stages to avoid local minima: the first encompasses a search for an initial model in the vicinity of the global minimum of the cost function using a stochastic approach. In Cary and Chapman (1988), this stage also included a traveltimes criterion for model selection, which we do not use. The second stage uses the model found in the first stage as the starting point for a gradient-based constrained optimization. The solution of the optimization problem can then be found using a range of algorithms such as Levenberg-Marquardt or sequential quadratic programming (Nocedal and Wright, 1999). Due to the speed of the computations of WKBJ seismograms, the target-oriented inversion described above can be repeated many times to obtain different realizations of the inverted model parameters. Hence, it provides a means for the estimation of the statistical distribution of the inverted parameters.

Data preconditioning includes convolution with the same boxcar filter (equation 4) used to produce the WKBJ synthetics to ensure the same smoothing. If appropriate, preprocessing may include elimination of possible ground roll and multiple reflections. Because this method is target-oriented, outside a window of interest centered on the target reflection the input data are muted after being bandpassed to a suitable frequency range.

Depending on the input data, two different misfit functions may be used during the inversion: one based on least-squares differences between waveforms and another based on least-squares differences of envelopes (modulus of the analytic signal of input traces).

The WKBJ synthetic seismograms $W(t, x_j)$ are computed by convolution with a predefined source signature $s(t)$ and the WKBJ Green function obtained from equation 5. Then, the residual vector is defined as $\mathbf{r} = \mathbf{d} - c\mathbf{w}$, where c is an overall scalar between the input data D and the synthetics W (or, alternatively, their envelopes D_e and W_e), both of which have been mapped into corresponding column vectors $\mathbf{d}$ and $\mathbf{w}$. Following Chapman and Orcutt (1985), we minimized the norm of $\mathbf{r}$, normalized by the energy in the input data, with the additional constraint that the scalar c is found as part of the least-squares problem, i.e., the objective function to be minimized is

$$E = 1 - \frac{\langle \mathbf{d}, \mathbf{w} \rangle^2}{\langle \mathbf{d}, \mathbf{d} \rangle \langle \mathbf{w}, \mathbf{w} \rangle}\,, \qquad (6)$$

Gradient computation during the local optimization stage also benefits from the low cost of producing synthetic WKBJ seismograms. The cost of computing WKBJ differential seismograms analytically is approximately the same as numerically for all the parameters, except for the differentials for the P-wave velocity below the target interface. In this case, numerical differencing of seismograms is cheaper, due to complications with integral evaluations near the critical slowness.

Results

The first part of this section refers to inversion tests done on a synthetic data set, while the second reports on inversions done on a shot-gather from the integrated seismic imaging and modeling of margins (iSIMM) project (Christie et al., 2006b).

Inversions on synthetic elastic models

Test inversions for isotropic models were done over the three-layered model shown in Table 1. The first layer corresponds to the overburden and the inversion aims at estimating parameters from the two bottom layers. Here, we did not consider overburden transmission effects, which would imply inclusion of reflection and transmission coefficients for the overburden in the computation of the propagation dyadic $\mathscr{G}_{\text{ray}}$ (equation 3).

Table 1: Parameters for three-layered model used in elastic inversions. Layer thickness is designed by Δz; P-wave velocity, V_P; shear-wave velocity, V_S; and density by ρ.

	Δz (km)	V_P (km/s)	V_P/V_S	ρ (g/cm^3)
layer 1	0.75	1.48	∞	1.0
layer 2	1.0	2.0	2.0	2.2
layer 3	∞	3.5	1.84	2.5

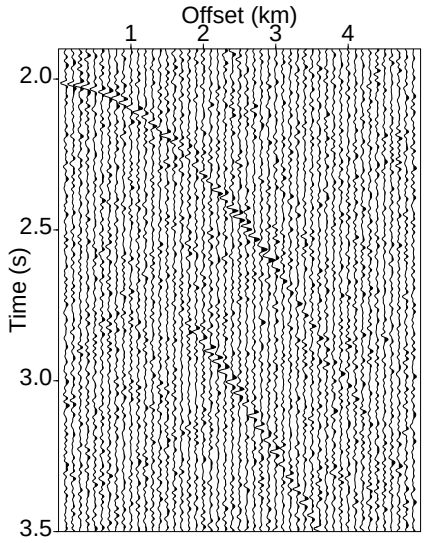

Figure 1: Data modeled with reflectivity algorithm using parameters from Table 1 with Gaussian noise added, the signal-to-noise ratio is 5.

The target reflection for the inversion tests is the event close to 2 s on the short offsets, with critical-angle reflection about 2.5 km offset (Figure 1). During the inversion the source wavelet was assumed to be known. The parameters being inverted for in this example are densities and V_P/V_S ratios in both layers 2 and 3 and the P-wave velocity in layer 3. Prior to inversion, the input traces were muted outside a boxcar window of about 100 ms, centered around the target reflection event. The objective function used waveforms to compute the misfit and the random search to find an initial model used, in each inversion, ten thousand different models spanning the parameter space shown in Table 2.

The summary of one hundred different realizations of the inversion is shown on Table 3. Interestingly, the results of all these inversions converged to the same answer in terms of velocity ratios and P-wave velocity, while they wandered about various values of density. Such behavior of the solutions demonstrates that one cannot determine the exact values of density in each layer, but can constrain the jump in density across an interface. Similarly, the contrast in velocity ratio offers more accurate estimations than individual layer values for this elastic model case.

Table 2: Range of parameters allowed in the inversion tests for synthetic elastic model. A Gaussian distribution is denoted by average $\pm$ one standard deviation notation. Otherwise the distribution is uniform, if a range of values is given.

parameter	layer 2	layer 3
V_P (km/s)	2.0	2.0 – 6.0
V_P/V_S	1.9 – 3.0	2.0 $\pm$ 0.25
ρ (g/cm^3)	1 – 3.5	1 –3.5
Δz (km)	1.0	∞

Table 3: Inversion results for the synthetic elastic model for 100 different realizations of the inversion (average $\pm$ one standard deviation). Contrasts between the layers denoted by Δ.

parameter	layer 2	layer 3
V_P (km/s)	N/A	3.477 $\pm$ 5E-04
V_P/V_S	1.90 $\pm$ 0.005	1.77 $\pm$ 0.005
ρ (g/cm^3)	2.28 $\pm$ 0.59	2.57 $\pm$ 0.66
$\Delta\rho$ (g/cm^3)	0.30 $\pm$ 0.08	
$\Delta V_P/V_S$	-0.13 $\pm$ 0.003	

iSIMM data

This point-receiver 2D seismic line—acquired between the Faroes and the Shetland islands—was chosen because it provided the opportunity to test the WKBJ-based inversion workflow on shot gathers that contained a clean refraction signal coming from the top of the basalt flows, found beneath the sedimentary section.

Figure 2 displays the shot gather used in the inversions. The target reflection is the event at 2.5 s with a strong refraction signal on long offsets. The source wavelet was obtained from the shot near-field hydrophone data, considering vertical propagation, and convolution with the corresponding source ghost. Note that, within the pass-band (7-15 Hz) used in the inversions, the wavelet extends for about 400 ms and is composed of three peaks, with a highest central peak delayed a 140 ms to the onset of the wavelet (Figure 2). Given such a long non-zero phase wavelet, the misfit function using envelopes rather than the waveforms proved more robust for this case.

Propagation through the overburden was accounted for only in terms of traveltimes by laterally averaging the 2D velocity model of Lau et al. (2010) between the shot and receivers up to 8km offset. The ranges for the model parameters during the inversions are shown in Table 4. Again, these ranges define the parameter space during the random global search stage of the inversion, and constrain the parameters during the gradient-based optimization stage. In this example, we invert for the six elastic parameters defining both layers ($V_P, V_P/V_S$ ratio and density) and the relative thickness of the layer above the target interface.

Figure 3 shows how the WKBJ synthetics from one of the

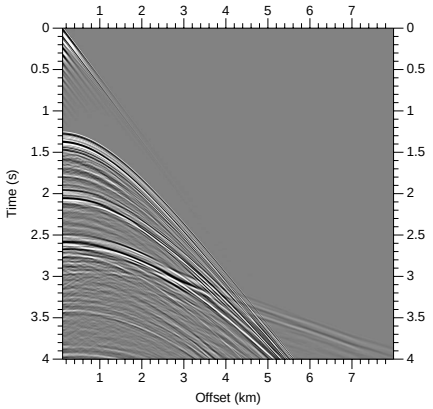

Figure 2: Shot from iSIMM data used in the inversions, with target reflection (top of basalt flows) at 2.5 on the nearest offset. The larger part of the refraction is due to a diving wave generated by strong vertical velocity gradient below the top of basalt flows

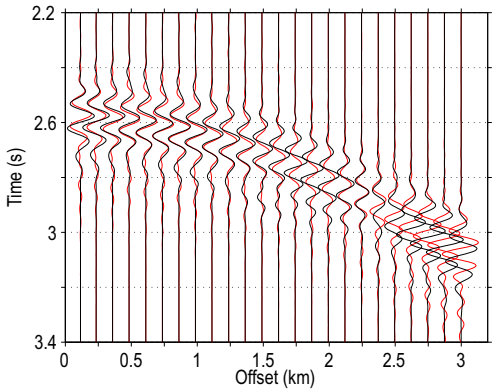

Figure 3: WKBJ (red) vs. iSMM (black) traces, top basalt reflection, no normalization.

Table 4: Range of parameters allowed in the inversion tests for the top basalt reflection.

parameter	sediments	basalt layer
V_P (km/s)	2.5 – 3.0	2.6 – 5.5
V_P/V_S	1.7 – 2.0	1.7 – 2.0
ρ (g/cm^3)	2.0 – 2.8	2.75 $\pm$ 0.25
Δz (km)	0.01 – 1.0	∞

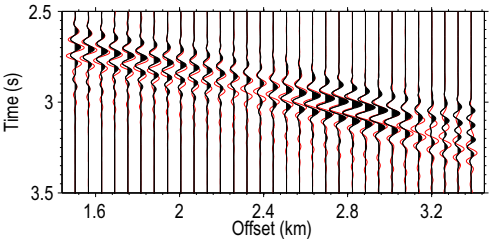

Figure 4: Inversion results close to the critical offset, with an offset-dependent time shift $t = p_r x$, where x is the offset relative to the first trace and $p_r = 0.03$ s/km , is a "reference" slowness.

inverted solutions are able to reproduce the offset variation of the amplitude observed in the data, with dimming from the short offsets to about 2.25 km, followed by a sharp increase in amplitude as the critical offset is reached between 2.5- and 3-km offset. The fit of the moveout only starts to deteriorate with offset beyond 2.5 km offset, stressing the limitations of fitting a 2D velocity field with a 1D earth model. Nevertheless, Figure 4 illustrates that using a single "reference" slowness p_r to make a local time shift $t = p_r x$, where x is offset, we can remove this moveout discrepancy and observe that the WKBJ synthetics and the data waveforms lie on top of each other.

The contrasts obtained from the inversion indicate a significant positive jump in P-wave velocity (1.45 $\pm$ 0.12 km/s) and density (0.79 $\pm$ 0.25 g/cm^3), associated with a slight drop in the V_P/V_S ratio (-0.09 $\pm$ 0.1), in agreement with our expectations given the geological model of sediments overlying basalt flows. Due to the lack of "ground truth" measurements, it is hard to assess whether these results are accurate. Incidentally, log data from the Lopra well (Christie et al., 2006a)—located in the Faroes Islands, about 60 km west of the 2D seismic line—show that densities and V_P/V_S at comparable stratigraphic levels in the basalt layer are close to those obtained in our inversion: 2.94 ± 0.18 g/cm^3 against the log average of 2.86 ± 0.35 g/cm^3; likewise, V_P/V_S is 1.81 $\pm$ 0.09 compared to average of 1.84 in the Lopra well.

Conclusions

Here we demonstrate the feasibility of using WKBJ seismograms to extend AVO-type inversions to long-offset reflection seismic data. By taking into account the curvature of the incident wavefront with the WKBJ modeling, one can synthesize non-geometric arrivals, like head waves, a feature that enables correct modeling of seismic traces in the vicinity of and beyond the critical angle. As a consequence, a larger range of offsets can be input into the inversion.

The test inversions made on the synthetic model used data before and after the critical angle and were able to recover not only the P-wave velocity below the interface, but crucially the jump in density and, albeit less accurately, the jump in the ratio of velocities. In addition, the inversion of top of basalt reflection offers a real-data example of how WKBJ seismograms can replicate amplitude variations of waveforms around the critical angle, adding confidence that such matching should improve reservoir parameter estimations with reflection seismic data. Therefore, we conclude that the WKBJ-based inversion improves the resolution of velocity and density contrasts in comparison with conventional AVO inversion based on pre-critical partial reflections.

Acknowledgements

We thank Schlumberger Cambridge Research Ltd. for permission to publish this work. We also thank S. Archer, R. Fletcher and J. Rickett for their comments and suggestions that helped to improve this abstract.

References

Aki, K. and P. G. Richards, 2002, Quantitative seismology: Sausilito: University Science Books.

Cary, P. W. and C. H. Chapman, 1988, Automatic 1-D waveform inversion of marine seismic refraction data: Geophysical Journal, **93**, 527–546.

Chapman, C. H., 1978, A new method for computing synthetic seismograms: Geophysical Journal of the Royal Astronomical Society, **54**, 481–518.

———, 2004, Fundamentals of seismic wave propagation: Cambridge University Press.

Chapman, C. H. and J. A. Orcutt, 1985, Least-squares fitting of marine seismic refraction data: Geophysical Journal of the Royal Astronomical Society, **82**, 339–374.

Christie, P., I. Gollifer, and D. Cowper, 2006a, Borehole seismic studies of a volcanic succession from the Lopra-1/1a borehole in the Faroe Islands, nothern North Atlantic: Geological Survey of Denmark and Greenland Bulletin, **9**, 23–40.

Christie, P. A. F., Z. C. Lunnon, R. S. White, N. Kusznir, A. Roberts, A. W. Roberts, C. Parkin, L. Smith, J. Eccles, D. Healy, N. Hurst, V. Tymms, A. Chappell, and R. Fletcher, 2006b, iSIMM experience with peak- and bubble-tuned sources for generating low frequencies: 68th EAGE Conference & Exhibition, Extended Abstracts, Z–99, EAGE.

Lau, K. W. H., R. S. White, and P. A. F. Christie, 2010, Integrating streamer and ocean-bottom seismic data for sub-basalt imaging on the Atlantic Margin: Petroleum Geoscience, **16**, 349–366.

Nocedal, J. and S. J. Wright, 1999, Numerical optimization: Springer-Verlag.

Rüger, A., 1997, P-wave reflection coefficients for transversely isotropic models with vertical and horizontal axis of symmetry: Geophysics, **62**, 713–722.

Shuey, R. T., 1985, A simplification of the Zoeppritz equations: Geophysics, **50**, 609–614.

Ursenbach, C. P., A. B. Haase, and J. E. Downton, 2007, An efficient method for AVO modeling of reflected spherical waves: Journal of Seismic Exploration, **16**, 79–104.

van der Baan, M. and D. Smit, 2006, Amplitude analysis of isotropic P-wave reflections: Geophysics, **71**, C93–C103.